Available online at www.sciencedirect.com
SCIENCE DIRECT®
Journal of Solid State Chemistry 171 (2003) 30–37
JOURNAL OF SOLID STATE CHEMISTRY
http://elsevier.com/locate/jssc

Nanocrystalline $LaNi_5$-type electrode materials for Ni-MH_x batteries

M. Jurczyk,[a,*] L. Smardz,[b] K. Smardz,[a] M. Nowak,[a] and E. Jankowska[c]

[a] *Institute of Materials Science and Engineering, Poznan University of Technology, Sklodowska Curie 5 Sq., 60-965 Poznan, Poland*
[b] *Institute of Molecular Physics, Polish Academy of Sciences, Smoluchowskiego 17 St., 60-179 Poznan, Poland*
[c] *Central Laboratory of Batteries and Cells, Forteczna 12/14 St., 61-362 Poznan, Poland*

Received 23 April 2002; received in revised form 22 July 2002

Abstract

$LaNi_5$-based hydrogen storage alloys are a promising choice for hydrogen energy systems. In this work, nanocrystalline La(Ni,M)$_5$ (M = Mn, Al, and Co) alloys have been synthesized by mechanical alloying (MA) followed by annealing. The discharge capacity of electrodes prepared by application of MA and annealed $LaNi_5$ alloy powder is low. It was found that the partial substitution of Ni by Al or Mn in La(Ni,M)$_5$ alloy leads to an increase in discharge capacity. On the other hand, cobalt substituting nickel in $LaNi_{4-x}Mn_{0.75}Al_{0.25}Co_x$ greatly improves the cycle life of this material. For $x=0.25$ the discharge capacities up to $\sim 260\,mAh\,g^{-1}$ were measured at current density of charging and discharging of $i=40\,mA\,g^{-1}$. The studies show that electrochemical properties of Ni–MH_x batteries are a function of chemical composition and microstructure of the electrode materials used. XPS studies showed that the shape of the valence band measured for the arc-melted (polycrystalline) $LaNi_5$ is practically the same as that reported earlier for the single crystalline sample. The substitution of Ni by Al in $LaNi_5$ leads to significant modifications of the electronic structure of the polycrystalline sample. Furthermore, the XPS valence band of the MA nanocrystalline $LaNi_4Al_1$ alloy is considerably broader compared to that measured for the polycrystalline sample. The strong modifications of the electronic structure and the significant surface segregation of lanthanum atoms in the MA nanocrystalline $LaNi_5$-type alloys could significantly influence its hydrogenation properties.

Keywords: Rare-earth compounds; Mechanical alloying; Electrode materials; XPS; AES; Nanostructure

1. Introduction

There is considerable concern over global warming and measures will have to be taken to slow down the build-up of green house gases in the atmosphere. Pollution and increasing need for energy sources prompt research of clean and safe energy systems with high-energy density [1].

In recent years, hydride forming intermetallics have become increasingly important because of their widespread application in metal-hydride storage materials/batteries [1–6]. However, either low storage capacity by weight or poor absorption–desorption kinetics in addition to a complicated activation procedure, have limited the practical use of metal hydrides. To be useful for storing hydrogen the material should: be capable of storing large quantities of hydrogen, be readily formed and decomposed, have reaction kinetics satisfying the charge–discharge requirements of the system, have the capability of being cycled without alteration in pressure–temperature characteristics during the life of the system, have low hysteresis, have good corrosion stability, have low cost, and be, at least, as safe as other energy carriers.

Conventionally, the polycrystalline hydride materials have been prepared by arc melting and annealing. The $LaNi_5$ alloy, which crystallizes in the hexagonal $CaCu_5$-type structure can absorb up to 5.5 H/f.u. at room temperature. The merit of $LaNi_5$-type compounds is that they exhibit low hysteresis, are tolerant to gaseous impurities and are easily hydrogenated in the initial cycle after manufacture. The properties of hydrogen host materials can be modified substantially by alloying, to obtain the desired storage characteristics, e.g. proper capacity at a favorable hydrogen pressure. It was found that the partial respective replacement of Ni in $LaNi_5$ by small amounts of Al, Mn, Si, Zn, Cr, Fe, Cu, or Co altered the hydrogen storage capacity, the stability of

*Corresponding author. Fax: +48-61-665-3576.
E-mail address: jurczyk@sol.put.poznan.pl (M. Jurczyk).

0022-4596/03/$ - see front matter © 2002 Elsevier Science (USA). All rights reserved.
doi:10.1016/S0022-4596(02)00142-1

the hydride phase and the corrosion resistance [7–9]. Generally, in the transition metal sublattice of $LaNi_5$-type compounds, substitution by Mn, Al, and Co has been found to offer the best compromise between high hydrogen capacity and good resistance to corrosion [10].

Recently, Iwakura et al. investigated the effect of partial displacement of cobalt for nickel by measuring the crystallographic, thermomagnetic and kinetic properties of hydrogen storage alloys in the composition range of polycrystalline $MmNi_{4.0-x}Mn_{0.75}Al_{0.25}Co_x$ ($0 \leqslant x \leqslant 0.6$) [11]. Increase in cobalt content of the alloys, due to the enlargement of the unit cell volume, stabilizes the resulting hydride and improves the cycling durability without a decrease in discharge capacity.

Substantial improvements in the hydriding–dehydriding properties of metal hydrides could possibly be achieved by formation of nanocrystalline structures by non-equilibrium processing techniques such as mechanical alloying (MA), high-energy ball-milling (HEBM) or reactive milling (mechanically induced gas–solid reactions) [4–6,12–14]. The use of these techniques is very effective in lowering the cost of hydrogen storage materials. It has been shown that ball milling of $LaNi_5$ is effective for the improvement of the initial hydrogen absorption rate, due to the reduction in the particle size and to the creation of new clean surfaces [13]. Proper engineering of microstructure and surface by using unconventional processing techniques will lead to advanced nanocrystalline intermetallics representing a new generation of metal hydride materials.

Recently, mechanical alloying has been used to make a nanocrystalline TiFe-, ZrV_2- and $LaNi_5$-type alloys [4–6,12–14]. As shown in our earlier work, nanocrystalline $MmNi_{3.5}Al_{0.8}Co_{0.7}$ powder has a larger capacity than the amorphous parent alloy material [5]. Annealing leads to grain growth, release of microstrain and to an increase of the storage capacity [13]. This behavior is due to a well-established diffusion path for hydrogen atoms along the numerous grain boundaries [12].

In order to optimize the choice of the intermetallic compounds for a selected application, a better understanding of the role of each alloy constituent on the electronic properties of the material is crucial. Several semi-empirical models [15,16] have been proposed for the heat of formation and heat of solution of metal hydrides and attempts have been made for justifying the maximum hydrogen absorption capacity of the metallic matrices. These models have shown that the energy of the metal–hydrogen interaction depends both on geometric and electronic factors. However, to date, studies of electronic properties of hydrides of complex system are rather limited and cannot yet provide an answer to these interesting questions.

In this work, the influence of chemical composition on the structural and electrochemical properties of nanocrystalline $La(Ni,M)_5$-type alloys, prepared by mechanical alloying (MA) and followed by annealing, was investigated (M = Al, Mn, and Co). The electronic properties of polycrystalline and nanocrystalline $La(Ni,Al)_5$ alloys were studied using X-ray photoelectron spectroscopy (XPS). The nanocrystalline materials with an addition of 10 wt% an Ni powder, were subjected to electrochemical measurements as working electrodes. These measurements may supply useful indirect information about the influence of the chemical and electronic structures of polycrystalline and nanocrystalline $LaNi_5$-type alloys on their electrochemical properties.

2. Experimental details

The nanocrystalline $LaNi_5$-type alloys were prepared using mechanical alloying followed by annealing. Mechanical alloying was performed under an argon atmosphere using a SPEX 8000 D Mixer Mill. The round bottom stainless vials were used. The purity of the starting metallic elements La, Ni, Mn, Al, and Co was 99.9, 99.9, 99+, 99.95, and 99.8 wt%, respectively. The composition of the starting powder mixture corresponded to the stoichiometry of the "ideal" reactions with an extra 8 wt% of lanthanum. The elemental powders (La: $\leq$425 μm; Ni: 3–7 μm; Mn: $\leq$45 μm; Al: $\leq$75 μm; Co: 2 μm) were mixed and loaded into the vial in the glove box (Labmaster 130) containing an argon atmosphere ($O_2 \leq 2$ ppm and $H_2O \leq 1$ ppm). The mill was run up to 40 h for every powder preparation. The as-milled powders were heat treated at 700°C for 0.5 h under high purity argon to form hexagonal $CaCu_5$-type phase. The powders were examined by XRD analysis, using Co$K\alpha$ radiation, at various stages during mechanical alloying, prior to annealing and after annealing. Independently, the MA process of the $LaNi_5$-type mixtures has been studied by scanning electron microscopy (SEM) and transmission electron microscopy (TEM). TEM and SEM were performed with a Philips EM 300 and Joel JSM-50A, respectively. To prepare the TEM specimens, the alloy powders were first rolled between Al plates, mechanically polished to thin films of thickness of 50 μm and ion milled. The crystallization behavior of the mechanically alloyed materials was examined by differential scanning calorimetry (DSC 404, Netzsch). Typical crystallite sizes, D_{hkl}, were estimated from the half-width of lines using the Scherrer equation: $D_{hkl} = 0.91 \times \lambda/\beta \cos\theta$, where λ is the X-ray wavelength, β is the peak width at half-maximum peak high (radians), and θ is the position of the peak. The change in the structure of powdered samples was observed using atomic force microscope (Nanoscope IIIa—Digital Instruments, USA) [14].

The polycrystalline $LaNi_5$ and $LaNi_4Al_1$ alloys were prepared by arc-melting stoichiometric amounts of the

constituent elements (purity 99.9% or better) in a high-purity argon atmosphere. The as-cast ingots were homogenized at 900°C for 3 days and then cooled to room temperature in water.

The bulk chemical composition of the samples was measured under environmental conditions by X-ray fluorescence (XRF) method. The surface chemical composition and the cleanness of the samples were measured in ultra high vacuum (UHV) using XPS and Auger photoelectron spectroscopy (AES). The MA powder for XPS and AES measurements was cold pressed to a pellet in an argon atmosphere. Before loading into the UHV preparation chamber, the sample of studied material with well-polished surface was rinsed with twice-distilled water and dried in air. In the preparation chamber (10^{-7} Pa) the sample was mounted on a holder equipped with a heater using a special transfer system. The sample was first heated in the preparation chamber (base pressure 10^{-7} Pa) at 150°C for 3 h and then in situ transferred to the analysis chamber (base pressure 4×10^{-9} Pa) for the XPS measurements. The sample surface was cleaned by ion (Ar^+, 3 keV) bombardment until the oxygen and carbon free surface of the sample was obtained. The above UHV heating procedure at relatively low temperature does not change the microstructure of the studied samples. This is revealed by the ex situ XRD studies.

The XPS spectra were measured at room temperature (RT) using a SPECS EA 10 PLUS energy spectrometer with Al$K\alpha$ radiation (X-ray spot size $\sim1\times4\,mm^2$) of 1486.6 eV. The energy spectra of the electrons were analyzed by a hemispherical analyzer ($FWHM_{Mg}K\alpha=0.8$ eV for Ag $3d_{5/2}$).

Selected samples were also analyzed with depth-profiling AES [17]. In this experiment the electron beam (average diameter ~0.1 mm, electron-gun STEIB) with $E_p=3$ keV and $I_p=1$ mA was incident at an angle of 43° to the surface of the sample. The surface layer of the studied sample could be removed using a differentially pumped SPECS ion gun etching system. We have used a 3 keV Ar^+ ion beam that was incident at an angle of 45° to the surface of the sample.

The mechanically alloyed and annealed (nanocrystalline) materials with an addition of 10 wt% Ni powder, were subjected to electrochemical measurements as working electrodes after pressing (under 80 kN cm^{-2}) into a 0.5 g pellet formed between nickel nets acting as current collector. The diameter of each electrode was 10.4 mm and the thickness approximately 1.4 mm. Soaking of the electrodes in 12 M KOH solution for 1 h at room temperature with additional etching at 100°C for 10 min in the same solution was sufficient for initial activation. The electrochemical properties of the electrodes were measured in a three-compartment glass cell, using a much larger $NiOOH/Ni(OH)_2$ counter-electrode and a Hg/HgO/6 M KOH reference electrode. All electrochemical measurements were carried out in deaerated 6 M KOH solution prepared from Analar grade KOH and 18 MΩ cm^{-1} water, at 20°C. Potentiodynamic and galvanostatic techniques with either short- or long-term pulses using a conventional apparatus were applied to study the charge–discharge kinetics of the electrodes. A detailed description of the electrochemical measurements is given in Refs. [5,6].

3. Results and discussion

The results of the MA process have been studied by X-ray diffraction, microstructural investigations, AFM as well as by electrochemical measurements. Fig. 1 shows a series of XRD spectra of mechanically alloyed La–Ni powder mixture (0.3212 wt% La + 0.6788 wt% Ni) subjected to milling in increasing time. The originally sharp diffraction lines of La and Ni (Fig. 1a) gradually become broader and their intensity decreases with milling time. The peak broadening represents a reduction in the crystallite size and an increase in the internal strain in the MA material. The powder mixture milled for more than 30 h, has transformed completely to the amorphous phase ("X-ray amorphous" [18]), without formation of another phase (Fig. 1b). Using the La–Ni mixture composition, as the material example, the behavior of grain size of the crystallites has been studied during the mechanical alloying process. The Ni (111) diffraction line remains visible up to 20 h of milling. This allows an estimation of the change in the crystallite size of Ni with increasing milling time. The crystallite size decreases strongly from 50 nm at the

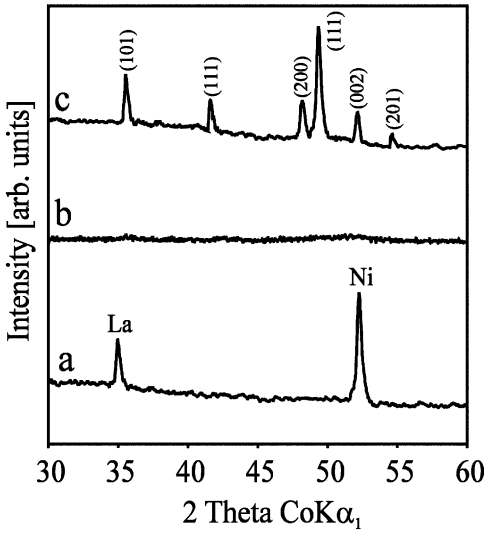

Fig. 1. XRD spectra of a mixture of La and Ni powders mechanically alloyed for different times in an argon atmosphere: (a) initial state (elemental powder mixture), (b) after MA for 30 h, and (c) heat treated at 700°C for 0.5 h.

beginning of the mechanical alloying process. The final size of crystallites, about 20 nm, seems to be favorable for the formation of an amorphous phase, which develops at the La–Ni interfaces. Further milling significantly weakens the diffraction peak intensity so that it was impossible to estimate the crystallite size. Formation of the nanocrystalline alloy was achieved by annealing of the amorphous material in high-purity argon atmosphere at 700°C for 0.5 h (Fig. 1c). All diffraction peaks were assigned to those of the hexagonal crystal structure of $CaCu_5$-type with cell parameters $a = 5.010$ Å and $c = 3.972$ Å. Table 1 reports the cell parameters of the studied materials. The unit cell volume of nanocrystalline $LaNi_{4-x}Mn_{0.75}Al_{0.25}Co_x$ system increased with the increase in cobalt content. The same results were obtained in the case of polycrystalline $MmNi_{4-x}Mn_{0.75}Al_{0.25}Co_x$ materials ($0 \le x \le 0.6$) [11].

The SEM technique was used to follow the changes in size and shape of the mechanically alloyed La–Ni powder mixture as a function of milling time (Fig. 2A). The microstructure that forms during MA consists of layers of the starting material. The thickness of the material decreases with the increase in mechanical alloying time leading to true alloy formation [19]. The sample shows cleavage fracture morphology and inhomogeneous size distribution. According to AFM studies, the average size of amorphous La–Ni powders was of order of 25 nm. Microstructural investigation of nanocrystalline $LaNi_5$ alloy by TEM is shown in Fig. 2B. The mean crystallite sizes were less than 35 nm.The annealing results in grain growth, as was observed earlier in the case of other nanocrystalline ZrV_2-type materials [5]. The mean crystallite sizes of the arc melted and homogenized samples were less than 1000 nm.

The amorphization process of $LaNi_5$ sample was also examined by DSC (Fig. 3). After 30 h of mechanical alloying of La–Ni mixture, the DSC curve stabilized exhibiting one exothermic effect at around 320°C. Taking into account the XRD results, one can assume that this effect is attributed to the crystallization of the amorphous phase formed by MA process.

Results on XRF measurements under environmental conditions revealed the assumed bulk chemical composition of the polycrystalline and nanocrystalline

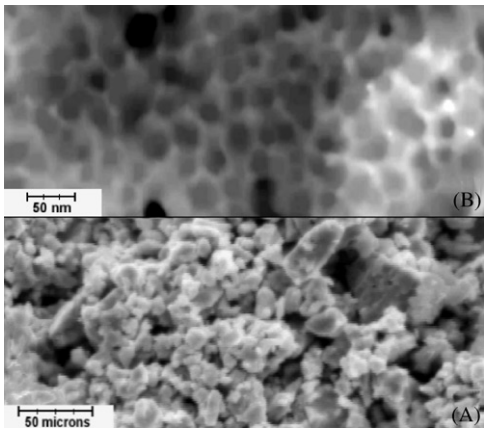

Fig. 2. SEM image of a mixture of La and Ni powders mechanically alloyed for 30 h under argon atmosphere (A) and TEM image of nanocrystalline $LaNi_5$ sample, bright field image (B).

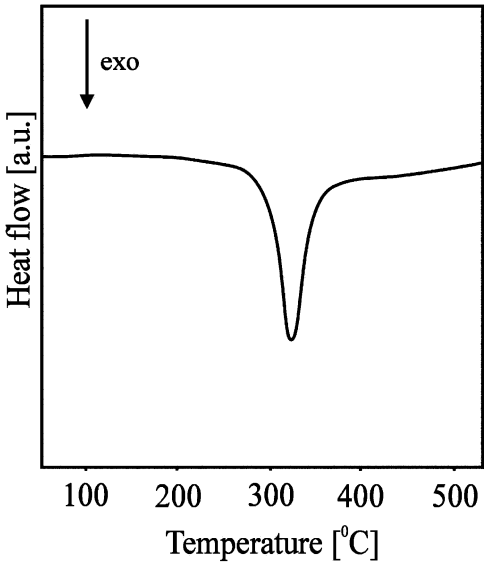

Fig. 3. DSC curve for an amorphous La–Ni mixture after 30 h mechanical alloying (heating rate in argon: 20°C min^{-1}).

Table 1
Structural parameters and discharge capacities for nanocrystalline $LaNi_5$-type materials (current density of charging and discharging was 40 mA g^{-1})

Composition	a (Å)	c (Å)	Discharge capacity (mA h g^{-1})	
			1st cycle	10th cycle
$LaNi_5$	5.010	3.972	84	97
$LaNi_4Al_1$	5.058	4.008	223	215
$LaNi_4Co_1$	5.011	3.975	39	114
$LaNi_4Mn_1$	5.015	4.005	239	212
$LaNi_4Mn_{0.75}Al_{0.25}$	5.073	4.040	243	218
$LaNi_{3.75}Mn_{0.75}Al_{0.25}Co_{0.25}$	5.075	4.039	258	242
$LaNi_{3.5}Mn_{0.75}Al_{0.25}Co_{0.5}$	5.076	4.041	254	233
$LaNi_{3.25}Mn_{0.75}Al_{0.25}Co_{0.75}$	5.078	4.043	227	201
$LaNi_3Mn_{0.75}Al_{0.25}Co_1$	5.080	4.045	219	217

$LaNi_5$-type compounds. In this method the information depth is a few micrometers. Therefore, the chemical composition determined by XRF measurements is characteristic for the whole sample. However, due to the environmental conditions in which experiment is performed, it is practically impossible to determine the level of impurities, such as oxygen, carbon and many others. Furthermore, the XRF set-up used in our experiment only allows us to measure elements with atomic number greater than 13. Due to the above-mentioned limitations of the XRF method, we have performed surface sensitive AES measurements under UHV conditions. The probing depth of the AES method is about 3 nm.Combining AES measurements with ion gun etching procedure, it was also possible to perform depth-selective chemical composition measurements. In addition, the AES measurements performed under UHV conditions allow us to determine the impurity levels (mainly for oxygen and carbon) of the samples.

Fig. 4 shows the element specific Auger intensities of the polycrystalline $LaNi_4Al_1$ sample as a function of the sputtering time, converted to depth. On the left-hand side is the top of the sample and on the right-hand side is the interior of the sample (not shown in Fig. 4). Shown are the peak-to-peak intensities of lanthanum, nickel, aluminum, oxygen, and carbon. As can be seen, there is a relatively high concentration of carbon and oxygen immediately on the surface, which could be mainly due to adventitious hydrocarbons. The carbon concentration strongly decreases towards the interior of the sample. At the metal interface itself only oxygen is present, making it very likely that only an oxide layer is formed and no other compounds, the latter growing apparently with a lower probability. We have found that at the oxide–metal interface mainly lanthanum and nickel are present. Taking into account that the escape-depth of the Auger electron from nickel and aluminum atoms is about 2 nm, the concentration of these elements on the metallic surface is significantly lower compared to the average bulk composition. Therefore, the lanthanum atoms, which segregate to the surface form a La-based oxide layer under atmospheric conditions. The oxidation process is depth limited such an oxide-covering layer with a well-defined thickness is formed by which the lower lying metal is prevented from further oxidation. In this way, one can obtain a self-stabilized oxide–metal structure. From the peak-to-peak amplitude we have calculated a maximum atomic concentration of oxygen inside the sample as 2 at%. The concentration of carbon impurities inside the sample was below 0.5 at%.

In Fig. 5 we show the element-specific Auger intensities of the nanocrystalline $LaNi_4Al_1$ sample as a function of the sputtering time, converted to depth. On the left-hand side is the top of the sample and on the right-hand side is the interior of the sample holder (not

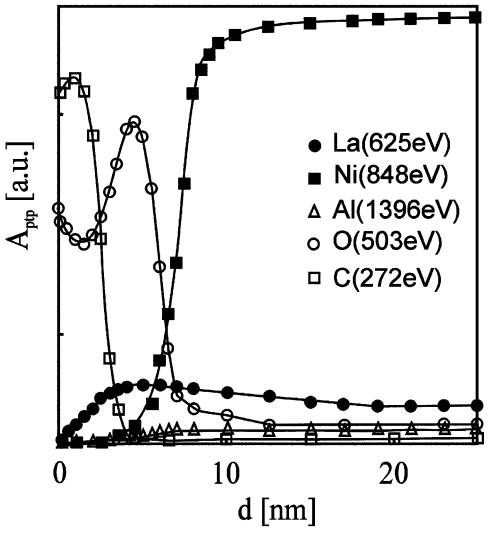

Fig. 4. Auger electron spectrum of polycrystalline $LaNi_4Al_1$ alloy versus sputtering time, as converted to depth. Shown are the peak-to-peak intensities of lanthanum, nickel, aluminum, oxygen, and carbon. The sample surface was not cleaned in UHV and is located on left-hand side.

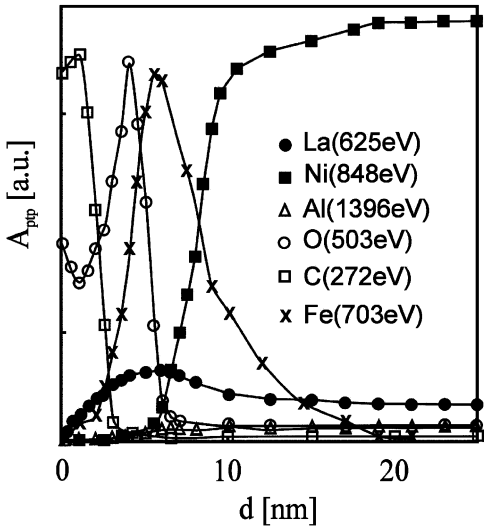

Fig. 5. Auger electron spectrum of nanocrystalline $LaNi_4Al_1$ alloy versus sputtering time, as converted to depth. Shown are the peak-to-peak intensities of lanthanum, nickel, aluminum, oxygen, carbon and iron. The sample surface was not cleaned in UHV and is located on left-hand side.

shown in Fig. 5). Shown are the peak-to-peak intensities of lanthanum, nickel, aluminum, oxygen, carbon, and iron. Similar to the results obtained for the polycrystalline sample (Fig. 4), there is a relatively high concentration of carbon and oxygen immediately on the surface. The carbon concentration strongly decreases towards the interior of the sample. We have found that at the oxide–metal only iron impurities and lanthanum atoms

are present. As the escape-depth of the Auger electrons from nickel and aluminum atoms is about 2 nm, we conclude that these elements are practically not present on the metallic surface. In other words, lanthanum atoms and iron impurities strongly segregate to the surface and form an oxide layer under atmospheric conditions. The lower lying Ni atoms form a metallic subsurface layer and are responsible for the observed high hydrogenation rate in accordance with earlier findings [20].

The AES results shown in Fig. 5 could be explained by a strong segregation of the Fe impurities and La atoms to the surface of the nanocrystalline $LaNi_4Al_1$ alloy. The segregation process of the La atoms is stronger compared to that observed for the polycrystalline sample. The presence of a significant amount of iron atoms in the surface layer of the nanocrystalline $LaNi_4Al_1$ alloy could be explained by Fe impurities trapped in the mechanically alloyed powders from erosion of the milling media. The amount of the Fe impurities considerably decreases in the subsurface layer of the sample. The bulk concentration of Fe impurities determined by AES and XRF is below the detection limit. The strong segregation of the Fe atoms to the surface is probably caused by the annealing of the MA powder and/or annealing of the nanocrystalline sample in the preparation chamber. From the peak-to-peak amplitude we have estimated a maximum atomic concentration of oxygen as ~ 2 at% in the interior of the nanocrystalline sample.

The observed strong segregation of the Fe impurities and La atoms, and the practical absence of the Al atoms in the top surface layer of the nanocrystalline $LaNi_4Al_1$ alloy could considerably influence the hydrogenation process in such a type of materials, also. Photoemission studies [20] combined with measurements of the magnetic susceptibility showed that lanthanum segregates to the surface of the polycrystalline $LaNi_5$ alloy in the presence of O_2 or H_2O, and that Ni precipitates are formed during hydrogenation. This represents a self-restoring mechanism of the active surface, since the highly reactive La removes the oxygen and keeps the Ni metallic [20]. Dissociative chemisorption of hydrogen, which often is the rate determining step in the hydrogen absorption by oxidized metals, may then occur on the metallic Ni precipitates and on the metallic subsurface.

Before discussing the effect of the substitution at the Ni site on the electronic structure, we shall summarize the most important features of the XPS valence band of the reference compound $LaNi_5$. The XPS valence band of polycrystalline $LaNi_5$, is plotted in Fig. 6a. We have found very good agreement between experimental results (Fig. 6a) and ab initio LMTO calculations of the total density of states (DOS) [21]. The occupied part of the condition band is dominated by the Ni-3*d* states with a non-negligible bonding contribution of the La-5*d*

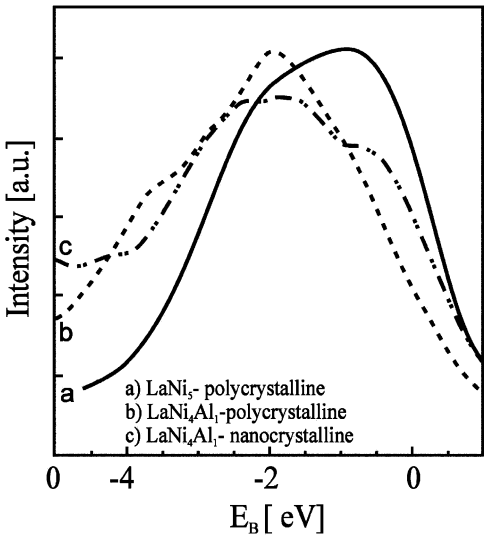

Fig. 6. XPS valence band spectra for polycrystalline $LaNi_5$ (a) and $LaNi_4Al_1$ (b) compounds as well as nanocrystalline $LaNi_4Al_1$ (c) using Al$K\alpha$ radiation. The polycrystalline samples were prepared by standard arc melting method. The nanocrystalline sample was prepared by mechanical alloying followed by annealing. The XPS measurements were performed immediately after heating in UHV conditions followed by removing of a native oxide and possible impurities layer using ion gun etching system (see text).

states. The main part of the La-5*d* states is located above the Fermi energy [21]. The XPS signal at E_F is high and mostly composed of Ni-3*d* states since the La-5*d* contribution is practically negligible [21]. In spite of the large value of the DOS at E_F $LaNi_5$ is paramagnetic. The valence band spectrum shown in Fig. 6a, measured for polycrystalline sample, is in very good agreement with the XPS measurements on single crystalline $LaNi_5$ [22].

Experimental XPS valence band spectrum of polycrystalline $LaNi_4Al_1$ alloy is shown in Fig. 6b. The corresponding structure of the valence band is significantly modified compared to that measured for the $LaNi_5$. In general, the lattice expansion associated with nickel substitution by aluminum could cause a narrowing of the Ni-3*d* subband due to a decrease in the Ni–Ni interaction. The above effect is manifested as a relatively sharp maximum of the valence band. On the other hand, the width of the valence band of the $LaNi_4Al_1$ alloy is greater in comparison with $LaNi_5$ system. This is due to the contribution of the Al *s* and *p* subbands, which are located near the bottom of the total valence band [21]. Furthermore, the experimental valence band shown in Fig. 6b could be also broader due to the effect of disorder caused by substitution of Ni by Al. The theoretical TB-LMTO calculations allow distinguishing between different contributions of the ions in the cell but the effect of disorder was neglected [21].

In Fig. 6c we show the XPS valence band of the nanocrystalline $LaNi_4Al_1$ alloy. The shape of the band is broader compared to that measured for the polycrystalline sample (see Fig. 6b). This is probably due to a strong deformation of the nanocrystals. Normally, the interior of the nanocrystals is constrained and the distances between atoms located at the grain boundaries expanded [23]. Note, that the surface layer with Fe impurities was removed before the XPS measurements and the oxygen concentrations in the nanocrystalline and polycrystalline samples are very similar. Therefore, the broadening of the valence band of the nanocrystalline $LaNi_4Al_1$ due to Fe or O impurities can be excluded.

Binary $LaNi_5$ crystallizes with the $CaCu_5$ structure type (space group $P6/mmm$) in which La occupies site 1(a) and Ni sites 2(c) and 3(g). The battery electrode material $LaNi_4Al_1$ is a substitutional derivative of $LaNi_5$ in which La occupies site 1(a) and Ni and Al sites 2(c) and 3(g) of space group $P6/mmm$. Experimental results have shown that the La sites do not accommodate Ni and Al atoms [24]. Furthermore, TB LMTO calculation [21] has shown that the impurity aluminum atoms prefer the 3g positions in agreement with experimental data [25]. However, in the case of MA nanocrystalline $LaNi_4Al_1$ alloy the Al atoms could also occupy metastable (2c) positions in the deformed grain. The above behavior could also modify the electronic structure of the valence band. As a result, the strong modifications of the electronic structure of the nanocrystalline $LaNi_4Al_1$ (Fig. 6c) compared to that of the polycrystalline sample (Fig. 6b) could significantly influence its hydrogenation properties.

The discharge capacity of an electrode prepared by application of MA and annealed $LaNi_5$ alloy powder is low (Table 1). It was found that the substitution of Ni by Al or Mn in La(Ni,M)$_5$ alloy leads to an increase in discharge capacity. The $LaNi_4Mn$ electrode, mechanically alloyed and annealed, displayed the maximum capacity at the first cycle but discharge capacity degraded strongly with cycling. On the other hand, alloying elements such as Al, Mn, and Co substituting nickel greatly improved the cycle life of $LaNi_5$-type material (Fig. 7, Table 1). With the increase of cobalt content in $LaNi_{4-x}Mn_{0.75}Al_{0.25}Co_x$, the material shows an increase in discharge capacity which passes through a wide maximum for $x = 0.25$. In nanocrystalline $LaNi_{3.75}Mn_{0.75}Al_{0.25}Co_{0.25}$ discharge capacities up to 258 mA h g^{-1} (at 40 mA g^{-1} discharge current) was measured.

Earlier, it was reported that the partial replacement of Al by Mn in polycrystalline $MmNi_{3.5}Co_{0.8}Al_{0.7-x}Mn_x$ significantly changed the metallurgical macrostructure [9]. The alloy containing Mn was characterized by equiaxed fine grains, high lattice strain and high pulverizing rate. In addition, a sputter deposition of the material containing Mn showed a higher discharge capacity and better rate capability than the Mn-free alloy. Moreover, cobalt in the alloy played a chemical role in the passivation of the alloy surface by the dissolution and precipitation (DP) processes and thereby improved the electrode performance [9]. Generally, alloying improves the alkali-resistance of Co, Mn and Al, controlling the rate of dissolution of $LaNi_5$-type electrode materials.

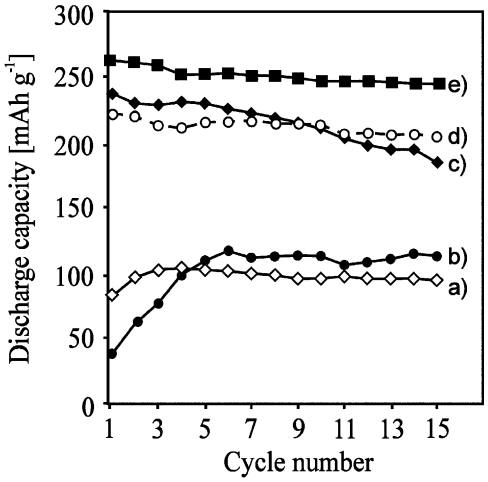

Fig. 7. Discharge capacities as a function of cycle number of $LaNi_5$-type negative electrodes made from nanocrystalline powders prepared by MA followed by annealing: (a) $LaNi_5$, (b $LaNi_4Co$, (c) $LaNi_4Mn$, (d) $LaNi_4Al$, (e) $LaNi_{3.75}Mn_{0.75}Al_{0.25}Co_{0.25}$ (solution, 6 M KOH; temperature, 20°C). The charge conditions were 40 mA g^{-1}. The cut-off potential versus Hg/HgO/6 M KOH was −0.7 V. Lines are provided as a guide to the eye.

The combination of a nanocrystalline La(Ni,Mn,Al,Co)$_5$ hydride electrode and a nickel positive electrode to form a Ni–MH_x battery has been successful. In the nickel sublattice of nanocrystalline $LaNi_5$, substitution of Mn, Al, and Co has been found to offer the best compromise between high discharge capacity and cycle life. Cobalt contained in the La(Ni,Mn,Al)$_5$ alloy gives the oxidized alloy surface a good electronic conductivity by a dissolution–precipitation process (surface coating), improving charging efficiency and preventing passivation. The cycle performance of a nickel–metal hydride battery was improved with cobalt content in La(Ni,Mn,Al)$_5$ alloy.

Very recently, we have also reported the pressure-composition isotherms for desorption of hydrogen from the gas phase, at 20°C, on nanocrystalline as well as polycrystalline $LaNi_{4.2}Al_{0.8}$ materials [26]. Results showed that the isotherms of nanocrystalline material differ significantly from the polycrystalline material, for which enhancement of solid-state solubility is observed. It was also observed that the amount of absorbed hydrogen at a pressure of 1.1 MPa decreases for nanocrystalline material. Furthermore, the plateau pressure was found to increase for nanocrystalline

material. The significant modification of the electronic structure of the nanocrystalline material (Fig. 6c) could be responsible for the observed hydrogenation properties. On the other hand, it is not excluded that another factor such as Fe impurities of MA samples due to degradation of milling media, could also influence on the hydrogenation process of nanocrystalline $LaNi_5$-type materials.

4. Conclusion

In this work, nanocrystalline $LaNi_5$, $LaNi_4M_1$ (M = Al, Co, and Mn) and $LaNi_{4-x}Mn_{0.75}Al_{0.25}Co_x$ ($x = 0$, 0.25, 0.5, 0.75, and 1.0) alloys synthesized by mechanical alloying and annealing were used as negative electrode materials for Ni–MH_x battery. The discharge capacity of an electrode prepared by application of MA and annealed $LaNi_5$ alloy powder is low. It was found that the partial substitution of Ni by Al or Mn in $La(Ni,M)_5$ alloy leads to an increase in discharge capacity. On the other hand, alloying elements such as Al, Mn, and Co substituting nickel greatly improved the cycle life of $LaNi_5$-type material. With the increase of cobalt content in $LaNi_{4-x}Mn_{0.75}Al_{0.25}Co_x$, the material shows an increase in discharge capacity which passes through a wide maximum for $x = 0.25$. The discharge capacities up to $\sim 260\,mAh\,g^{-1}$ were measured at current density of charging and discharging of $i = 40\,mA\,g^{-1}$.

The studies show, that electrochemical properties of Ni–MH_x batteries are the function of chemical composition and microstructure of used electrode materials. The substitution of Ni by Al in $LaNi_5$ leads to significant modifications of the electronic structure of the polycrystalline sample. On the other hand, the XPS valence band of the MA nanocrystalline $LaNi_4Al_1$ alloy is considerably broader compared to that measured for the polycrystalline sample. The strong modifications of the electronic structure and the significant surface segregation of lanthanum atoms in the MA nanocrystalline $LaNi_5$-type alloys could significantly influence its hydrogenation properties.

The combination of a nanocrystalline $La(Ni,Mn,Al,Co)_5$ hydride electrode and a nickel positive electrode to form a Ni–MH_s battery, has been successful. Therefore, the mechanical alloying is a suitable procedure for obtaining nanocrystalline $LaNi_5$-type alloy powders.

Acknowledgments

The financial support of the Polish National Committee for Scientific Research (KBN) under the Contract PBZ/KBN-013/T08/02 is gratefully acknowledged (www.inmat.pw.edu.pl/nanomaterialy/). One of us (M.N.) has been supported by the Fellowship from the Foundation for Polish Science (2002). The UHV equipment for surface analyses used for the AES measurements and glove box Labmaster 130 (M. Braun) was purchased by the Foundation for Polish Science under the programs SEZAM-1994 and TECHNO-2000, respectively.

References

[1] K. Hong, J. Alloys Compd. 321 (2001) 307.
[2] T. Sakai, M. Matsuoka, C. Iwakura, in: K.A. Gschneider Jr., L. Eyring (Eds.), Handbook on the Physics and Chemistry of Rare Earth, Vol. 21, Elsevier Amsterdam, 1995, pp. 135–180 (Chapter 142).
[3] J.J.G. Willems, K.H.J. Buschow, J. Kless-Common Met. 129 (1987) 13.
[4] A. Anani, A. Visintin, K. Petrov, S. Srinivasan, J.J. Reilly, J.R. Johnson, R.B. Schwarz, P.B. Desch, J. Power Sources 47 (1994) 261.
[5] M. Jurczyk, W. Majchrzycki, J. Alloys Compd. 311 (2000) 311.
[6] W. Majchrzycki, M. Jurczyk, J. Power Sources 93 (2001) 77.
[7] J. Kleparis, G. Wojcik, A. Czerwinski, J. Skowronski, M. Kopczyk, M. Beltowska-Brzezinska, J. Solid State Electrochem. 5 (2001) 229.
[8] D. Chartouni, F. Meli, A. Züttel, K. Gross, L. Schlapbach, J. Alloys Compd. 241 (1996) 160.
[9] T. Sakai, H. Miyamura, N. Kuriyama, H. Ishikawa, I. Uehara, Z. Phys. Chem. 183 (1994) 333.
[10] Z. Chen, Z. Chen, Y. Su, M. Lü, D. Zhou, P. Huang, Mate. Res. Bull. 33 (1998) 1449.
[11] C. Iwakura, K. Fukuda, H. Senoh, H. Inoue, M. Matsuoka, Y. Yamamoto, Electrochim. Acta 43 (1998) 2041.
[12] L. Zaluski, A. Zaluska, J.O. Ström-Olsen, J. Alloys Compd. 217 (1995) 245.
[13] G. Liang, J. Huot, R. Schulz, J. Alloys Compd. 320 (2001) 133.
[14] M. Jurczyk, E. Jankowska, M. Nowak, J. Jakubowicz, J. Alloys Compd. 336 (2002) 265.
[15] P.C. Bouten, A.R. Miedema, J. Less Common Metals 71 (1980) 147.
[16] RGriessen, T.Riesterer, in: L. Schlapbach, (Ed.), Topics in Applied Physics-Hydrogen in Intermetallic Compounds 1, Vol. 63, Springer, Berlin, 1988, p. 219, and references there in.
[17] L. Smardz, U. Köbler, W. Zinn, J. Appl. Phys. 71 (1992) 5199.
[18] C. Suryanarayana, Prog. Mate. Sci. 46 (2001) 1.
[19] J.S. Benjamin, Sci. Am. 40 (1976) 234.
[20] H.C. Siegmann, L. Schlapbach, C.R. Brundle, Phys. Rev. Lett. 40 (1978) 972.
[21] A. Szajek, M. Jurczyk, W. Rajewski, J. Alloys Compd. 307 (2000) 290.
[22] L. Schlapbach, Hydrogen in Intermetallic Compounds, II, Springer, Berlin, 1992, p. 165.
[23] M.R. Fitzsimmons, J.A. Estman, R.A. Robinson, A.C. Lawson, J.D. Thompson, R. Morshovich, Phys. Rev. B 48 (1993) 8245.
[24] E. Gurewitz, H. Pinto, M. Dariel, H. Shaked, J. Phys. F.: Metal Phys. 13 (1983) 545.
[25] J.M. Joubert, M. Latroche, A. Percheron-Guégan, F.B. Bourée-Vigueron, J. Alloys Compd. 275–277 (1998) 118.
[26] M. Jurczyk, K. Smardz, W. Rajewski, L. Smardz, Mat. Sci. Eng. A 303 (2001) 70.